of some approximations in the calculations. The corrections to $S(\psi,W)$ by Wegener are not valid for the entire range of β energies and angles, causing the final results for P_{11} to be somewhat too large in magnitude. The quoted errors in the final results are experimental statistical errors only. The average P_{11} from experiments two and three is $P_{11}=-0.024\pm0.015$.

Discussion

One notes that the polarization calculated from selected values of matrix elements, as described in the Introduction, was always negative. A positive polarization would be difficult to obtain from the theory since A_2 is measured to be negative. The final results of experiments two and three favor a slightly negative polarization and certainly preclude any unusually large effect outside the range predicted by Kotani's formulas.

The instabilities encountered during the long time of operation of the experiment are the factors that limit the precision of the result. Unless a particular transition shows a marked deviation from the Kotani approximation, this experiment does not appear to be a fruitful approach to the problem of delimiting the matrix elements.

ACKNOWLEDGMENTS

The communication of some unpublished calculations by Wegener on the multiple scattering of thin foils is appreciated. The help of N. S. Kendrick in the design and maintenance of some of the electronics is gratefully acknowledged.

PHYSICAL REVIEW VOLUME 152, NUMBER 3 16 DECEMBER 1966

Measurement and Analysis of the $^{90}Zr(d,p)^{91}Zr$ Reaction between 3.5 and 5.5 MeV

E. B. DALLY* AND J. B. NELSON†
Institut de Recherches Nucléaires, Strasbourg, France,
AND
WILLIAM R. SMITH‡
Oak Ridge National Laboratory, Oak Ridge, Tennessee,
and
Nuclear Physics Laboratory, Oxford, England,
(Received 1 August 1966)

The reaction $^{90}Zr(d,p)^{91}Zr$ is studied for the cases leading to ^{91}Zr in the ground state ($Q=4.98$ MeV) and the second ($Q=3.77$ MeV), the sixth ($Q=2.91$ MeV), and the eighth ($Q=2.42$ MeV) excited states. Results are presented for the incident deuteron energies 3.5, 4.0, 4.5, 5.0, and 5.5 MeV. At most energies there is a complete angular distribution ranging from 20° to 160° in steps of 10°. A distorted-wave Born-approximation analysis employing elastic-scattering parameters obtained from experiments in the region 11–16 MeV yielded good agreement with the angular shapes of the stripping data but not with their absolute magnitudes.

1. INTRODUCTION

MANY nuclear reactions are predominantly of the "direct" type.[1] Important among these are inelastic scattering of various projectiles and (d,p) and (d,n) stripping reactions. By "direct" is meant that at most only a few intermediate reaction modes are formed in going from the initial to the observed channel. Often, though, a description in which the entire reaction proceeds directly from the initial to the final channel is quite adequate. Such a mode is expressed mathematically by the distorted-wave Born approximation (DWBA). In the DWBA for (d,p) reactions, the transition is considered to be induced by the interaction between the neutron and the proton which together form the deuteron. The absorption and elastic scattering of the deuterons before the reaction and of the protons after the reaction are assumed to be explainable in terms of the same complex, spherically symmetrical potentials which describe the elastic scattering of deuterons and protons from the appropriate targets at the appropriate energies. It is not clear that the proton potentials should be exactly the same in stripping as in elastic scattering, but there has appeared no other basis for determining this potential. Therefore, it is of interest to nuclear spectroscopy to ascertain whether elastic proton potentials do yield good results when applied to stripping reactions.

The $^{90}Zr(d,p)^{91}Zr$ reaction in particular has been well accounted for by the DWBA in the energy range of 11

* Present address: High Energy Physics Laboratory, Stanford University, Stanford, California.
† Present address: Physics Department, University of Texas, Austin, Texas.
‡ Present address: Physics Department, University of Southern California, Los Angeles, California.
[1] W. Tobocman, *Theory of Direct Nuclear Reactions* (Oxford University Press, London, 1961).

to 15 MeV.[2–5] Several reasons for this success can be offered. The reaction channels are relatively weak compared to the elastic deuteron channel and the target is spherical and reasonably heavy, so that it should be describable by optical-model potentials. Also, the ^{91}Zr(p,n)^{91}Nb reaction has a low threshold and many low-lying levels through which the compound nucleus can decay by favored neutron emission. Thus the contribution of the compound nucleus reaction mode to any single (d,p) channel should be negligible.

A feature of the ^{90}Zr(d,p)^{91}Zr reaction which makes it useful for testing a direct reaction theory is that the spectroscopic factors corresponding to the ground state and the 1.21-MeV level of ^{91}Zr are already known[6] to have values near unity because of the closed-shell nature of ^{90}Zr.

This reaction is a good choice, then, to test the DWBA at bombarding energies lower than have usually been employed for heavier nuclei. Two factors make it plausible that the DWBA description is even better at energies well below the deuteron Coulomb barrier than above. First, at the lower energies the elastic cross section has gone up while the reaction intensity has decreased, so that the dominance of the elastic channel is enhanced. And second, the Coulomb repulsion of the deuterons should cause a larger percentage of the reaction to occur outside the bulk of the nuclear matter in the region where the theory should be the most reliable.

However, two practical difficulties exist which offset these advantages. An uncertain extrapolation of the elastic parameters from higher energies must be made, because of the energies under consideration the deuteron elastic-scattering angular distribution is almost a Rutherford one, and that for the proton is so simple in shape that it does not yield an unambiguous determination of the potential parameters. Also a very small contaminant of a light element in the target will yield protons which will obscure the protons emitted by the ^{90}Zr(d,p)^{91}Zr reaction.

The general conditions of the reaction are as follows. In the initial state, for the lower energies employed here, the deuteron tends to remain outside the nucleus because of the strong Coulomb repulsion. As the incident deuteron energy is increased, the deuteron starts to penetrate the nuclear surface. Thus, there is a gradual transition of the interaction mechanism in the initial state. On the other hand, the final state consists of the product nucleus ^{91}Zr in one of several excited states or the ground state, plus the proton, which because of the large Q values for the lower lying states, is well within the range of the nuclear potential.

In the next section we will describe the experimental methods employed to obtain the ^{90}Zr(d,p)^{91}Zr angular distributions and absolute cross sections corresponding to four levels in ^{91}Zr—the ground state (Q=4.98 MeV), and the second (Q=3.77 MeV), the sixth (Q=2.91 MeV), and the eighth (Q=2.42 MeV) excited states. The identification of the states corresponds to the scheme given in the Nuclear Data Tables. Figure 1 shows the level diagram of ^{91}Zr. (Reference 2 indicates an additional level at 2.35 MeV, just below the one that we identify as the eighth excited level.) Other low-lying states are not seen at all, are not resolved, or are present only weakly. The reactions have been studied at the bombarding energies 3.5, 4.0, 4.5, 5.0, and 5.5 MeV.

Following the next section will appear the details of the DWBA calculations and their comparison with the experimental results.

2. EXPERIMENTAL DETAILS

The deuteron beam was obtained from a High Voltage Engineering Corporation 5.5-MeV Van de Graaff accelerator. The beam ($\Delta E/E \leqslant 0.1\%$) entered the scattering chamber through a three-piece collimator, such that the smallest collimator produced a 1-mm-diam beam spot at the target. The scattering chamber contained a target holder and two movable arms for supporting detectors. The target and detector angles could be

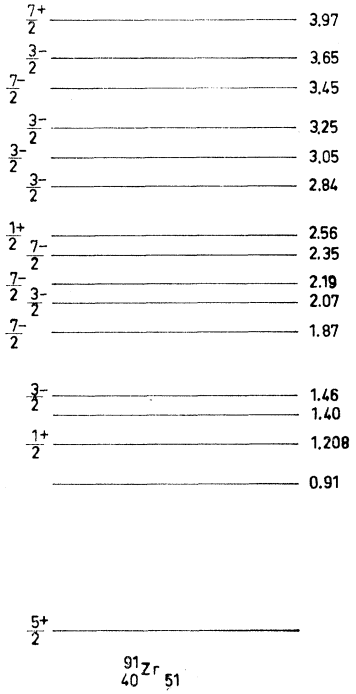

FIG. 1. Level scheme for ^{91}Zr. The spins and parities are those assigned in Ref. 2.

[2] B. L. Cohen and O. V. Chubinsky, Phys. Rev. **131**, 2184 (1963).
[3] R. L. Preston, H. J. Martin, Jr., and M. B. Sampson, Phys. Rev. **121**, 1741 (1961).
[4] J. K. Dickens, F. G. Perey, and R. J. Silva, Oak Ridge National Laboratory Report No. 3714, Vol. I, p. 4 (unpublished).
[5] W. R. Smith, Phys. Rev. **137**, B913 (1965).
[6] S. Ramavataram, Phys. Rev. **135**, B1288 (1964).

adjusted from outside the chamber. The alignment of the chamber was checked by counting the elastically scattered deuterons on each side of zero degrees as a function of angle.

Attached to the chamber, but insulated from it, was a Faraday cup. An Elcor Model A 309 A integrator was used, and was checked for stability with a standard current source and found to be reproducible to within $\pm\frac{1}{2}\%$. The use of the Faraday cup and the integrator served as a check on the performance of the monitor system (see below), and also as an independent measure of the absolute cross section.

The detector arrangement consisted of one to three solid-state detectors which were used to measure the angular distribution of the reaction, and one detector, always fixed at 90°, which was used to monitor all points by counting only elastically scattered deuterons. Elastic-scattering events were selected by a window amplifier. Because this elastic scattering could be related to Rutherford scattering (see below), the use of the monitor permitted the absolute calculation of the cross sections. In addition, with such a monitor, the results were independent of target angle and target nonuniformity. The monitor scaler was used to control the electronic circuitry by blocking the pulse-height analyzers and the integrator when a preset count was reached.

In order to confine the scattered particles to the sensitive surface of the detectors and to shield them from collimator spray at the small angles, a small holder with a double collimator was mounted in front of each detector. The angular resolution of the detectors was approximately 2°.

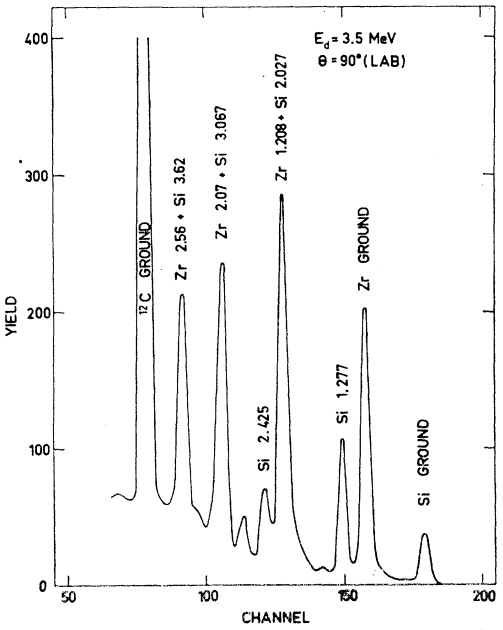

FIG. 2. Pulse-height spectrum for 3.5 MeV at 90°. Zirconium, carbon, and silicon reaction peaks are indicated.

A standard electronic arrangement consisting of an Ortec preamplifier and amplifier system was used with all detectors. Spectra were collected in R.I.D.L. and Intertechnique pulse-height analyzers. The electronic systems were checked on several different occasions for stability and linearity. A typical pulse-height spectrum taken during the experiment is shown in Fig. 2.

In studying the reactions it was necessary to make measurements in the presence of elastically scattered deuterons which are 10^5 and 10^6 times more frequent than the protons to be detected. When using a beam intensity of practical magnitude, the electronic systems are not fast enough to handle such a pulse rate without causing an excessive pile-up of pulses, which smears out the spectrum and also causes a large dead-time in the multi-channel analyzers. Thus, it was necessary to place absorbers between target and detectors to stop the deuterons but at the same time allow the higher-energy, lower-ionizing protons to pass through. The absorbers were mounted on a piece of aluminum in a slot directly behind the collimators. Aluminum absorbers of different thicknesses were calculated from the range tables of Williamson and Boujot.[7] No estimate of absorber uniformity was made, but the resolution of the spectra with absorbers for the different proton groups deteriorated such that the peaks were between 1.2 and 1.4 times broader than without absorbers. A ^{90}Zr target of purity 98.6% and of approximate thickness 1 mg/cm^2 was used throughout the experiment.[8] This target was rather thick, causing an energy loss to the deuteron beam of 100 keV at 3.5 MeV.

A contaminant in the target material gave additional strong peaks in the spectra for the 3.5-MeV points and less important ones at other energies. At certain angles the contaminant peaks moved under the zirconium reaction peaks, causing a large uncertainty in the analysis. Complete kinematic calculations for Si^{28} allowed the identification of all resolved levels. Silicon could be present in small mounts since zirconium is extracted from siliceous material, or could arise from the silicon found in diffusion pump oils. It could not be determined if the contaminant was surface deposited. Measured angular distributions of the reaction $Si^{28}(d,p)Si^{29}$ were found in the literature.[9–11] The silicon peaks are labeled in Fig. 2. The angular behavior of the clearly resolved contaminant peaks (usually those corresponding to the reaction leading to the ground

[7] C. Williamson and J. P. Boujot, Centre d'Etudes Nucléaires de Saclay, Rapport CEA No. 2189 (unpublished).
[8] E. L. Hudspeth, University of Texas, originally obtained from Oak Ridge National Laboratory (unpublished).
[9] D. Goss, Ph.D. thesis, University of Texas, 1964 (unpublished).
[10] J. A. Kuehner, E. Almqvist, and D. A. Bromley, Nucl. Phys. **21**, 555 (1960).
[11] H. S. Hausman, Ohio State University Van de Graaff Laboratory Report No. 1743, 1966, p. 16 (unpublished).

state or first excited state) agreed with the measured distributions of $Si^{28}(d,p)Si^{29}$. The intensities of silicon states lying under the zirconium groups were determined by normalizing to the resolved silicon states. This contribution was subtracted from the total number of counts found in the peak. No silicon cross sections were found at 4.5, 5.0, and 5.5 MeV. At these energies the relative silicon contributions were much weaker, and extrapolated estimates of the cross sections were used to make the corrections.

In addition to the silicon contaminant, contaminant peaks arising from surface-deposited carbon leading to the $C^{12}(d,p)C^{13}$ reaction interfered strongly with the measurements of the eighth level in the forward direction at 4.5, 5.0, and 5.5 MeV. Because these contaminant peaks were poorly resolved, and because only limited measured cross sections were found for this reaction,[12] the corrections for this contaminant were necessarily rather inaccurate, and as a consequence the assigned errors for these points are quite large.

Values of the cross section for the sixth level for the back angles at 4.5, 5.0, and 5.5 MeV are uncertain, owing to a contribution from the seventh level which was only partly resolved. Therefore the analysis of the data gives cross sections which might be somewhat high because of a poor subtraction of the seventh-level contribution.

The absolute reaction cross sections were determined in the following way. A detector, used as a monitor to measure the elastic-scattering yields, was set at 90° to the beam. A second detector, also set at 90°, was used to measure the reaction yields. The relative solid angles were determined from the ratio formed from the elastic-scattering yield found in each detector. Then absorbers were placed in front of the reaction detector and the reaction yields at 90° were measured at each energy for which angular distributions existed. This was done for a fixed amount of integrated beam charge. No changes in experimental variables were made from one energy to the next for these measurements. The center-of-mass cross sections calculated in this manner, as well as the errors, are shown in Table I.

To calculate the cross sections, the elastic scattering was assumed to be Rutherford scattering at 3.5 MeV. This assumption was checked by measuring the angular distributions of the elastic scattering for several energies. The shape was found to fit a Rutherford distribution to within the experimental uncertainties. These uncertainties arise from the statistics of the measurements made to verify the Rutherford distribution (1%) and the assigned upper limit of $\frac{1}{2}°$ for the uncertainty of the angle of scattering (2%). Optical-model calculations also gave a Rutherford distribution. In addition, angular distributions for elastic scattering

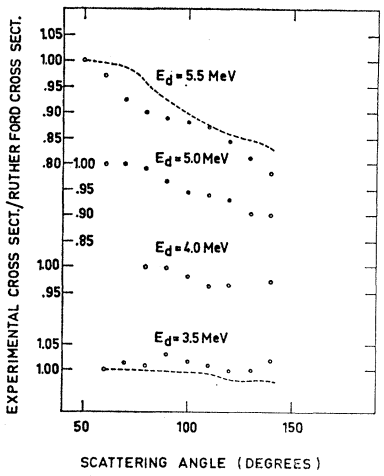

FIG. 3. Ratio of experimental elastic deuteron scattering cross section to Rutherford scattering cross section. The dashed curves at 5.5 and 3.5 MeV are the calculated results using parameter set A of Table II.

were measured at 4.0, 5.0, and 5.5 MeV. The ratio of the measured experimental to Rutherford yield for these energies is shown in Fig. 3. At 5.0 and 5.5 MeV, the ratio deviates from Rutherford scattering for angles greater than 80° and 60°, respectively. With this deviation taken into account, an independent calculation of the absolute reaction cross sections could be made. At each energy a measured solid-angle ratio was used, as well as the monitor and reaction yields. These results agreed with those shown in Table I, thus giving a satisfactory consistency check.

As a final consistency test, the cross sections for elastic scattering and the reactions were calculated using the measured value of the target thickness, integrated beam charge and solid angle. The results were consistently 12–15% smaller than the Rutherford cross section (or the cross section corrected for the deviation shown in Fig. 3). The reaction cross sections calculated in this manner were below the relative measurements by the same amount. The agreement between these values of the cross section is very good and the deviations from the relative values are easily accounted for by the uncertainty of the target thickness alone.

3. COMPUTATIONAL PROCEDURES

Neglecting constant factors, the $A(d,p)B$ stripping amplitude is proportional to[1]

$$\int dr_{dA} \int dr_{np} \phi(r_{pB}) \phi(r_{nA}) \times (V_{np} + V_{pA} - \bar{V}_{pB}) \phi(r_{np}) \phi(r_{dA}),$$

where the arguments of the relative wave functions indicate which two particles are involved, V_{np} and V_{pA} are interaction potentials, and $\bar{V}_{pb}$ is the averaged optical-model potential which determines $\phi(rB)$. As in

[12] N. I. Zaika, O. F. Nemets, and M. A. Tserineo, Zh. Eksperim. i Teor. Fiz. 39, 3 (1960) [English transl.: Soviet Phys.—JETP 12, 1 (1961)].

TABLE I. Experimentally measured cross sections for the reaction $^{90}Zr(d,p)^{91}Zr$. (Angles in degrees, center-of-mass cross sections in μb/sr. Total errors are given.)

	Ground state		Second excited state		Sixth excited state		Eighth excited state	
Lab angle	Center-of-mass angle	Cross section	Center-of-mass angle	Cross section	Center-of-mass angle	Cross section	Center-of-mass angle	Cross section
				3.5 MeV				
20	20.20							
30	20.29	6.26± 3	30.31	9.13± 2	30.33	0.845± 0.6		
40	40.37	10.6 ± 2	40.40	10.9 ± 2	40.43	1.69 ± 1.7		
50	50.44	16.2 ± 1	50.48	11.7 ± 3	50.51	4.62 ± 2.3		
60	60.50	16.7 ± 1	60.54	10.2 ± 1	60.57	12.2 ± 2.8		
70	70.54	18.1 ± 1	70.59	12.3 ± 1	70.62	15.1 ± 1	70.65	6.37± 1
80	80.57	16.8 ± 1	80.61	17.4 ± 1	80.65	15.4 ± 1.6	80.68	9.76± 1.1
90	90.58	17.8 ± 2	90.62	21.2 ± 2	90.66	19.1 ± 1.4	90.69	15.0 ± 1.5
100	100.57	19.4 ± 1	100.61	29.1 ± 2	100.65	22.1 ± 1.5	100.68	23.1 ± 2.4
110	110.54	22.7 ± 1	110.59	31.9 ± 2	110.62	33.2 ± 1.5	110.65	26.7 ± 3
120	120.50	24.4 ± 1	120.54	30.6 ± 2	120.57	32.5 ± 1.6	120.60	28.9 ± 2
130	130.44	23.5 ± 1	130.48	31.5 ± 1.6	130.51	37.0 ± 2	130.53	28.3 ± 1.5
140	140.37	23.1 ± 1	140.40	30.0 ± 1.4	140.43	35.7 ± 1.5	140.44	31.4 ± 2
150	150.29	22.0 ± 1	150.31	30.4 ± 2	150.33	33.0 ± 2.1	150.35	29.8 ± 1.6
160	160.20	21.8 ± 2	160.21	33.1 ± 2	160.23	35.4 ± 1.6	160.24	30.1 ± 1.7
				4.0 MeV				
20	20.20	18.3 ± 6	20.20	38.5 ±10	20.23		20.24	
30	30.30	14.1 ± 5	30.32	42.2 ± 7	30.34		30.35	
40	40.38	30.3 ± 3	40.41	43.1 ± 3	40.44	7.54 ± 2	40.46	
50	50.46	47.0 ± 3	50.49	40.9 ± 2	50.52	17.3 ± 2	50.54	
60	60.52	68.1 ± 3	60.56	33.8 ± 2	60.59	33.1 ± 3	60.61	31.3 ±10
70	70.56	69.6 ± 2	70.61	40.1 ± 2	70.64	50.9 ± 2	70.67	32.2 ± 2
80	80.59	66.2 ± 3	80.63	69.0 ± 3	80.67	52.9 ± 3	80.70	34.8 ± 3
90	90.60	63.5 ± 3	90.64	87.0 ± 4	90.68	70.3 ± 3	90.71	53.5 ± 4
100	100.59	71.0 ± 3	100.63	114 ± 3	100.67	90.3 ± 4	100.70	68.6 ± 4
110	110.56	79.7 ± 3	110.61	102 ± 4	110.64	104 ± 4	110.67	79.7 ± 4
120	120.52	75.9 ± 3	120.56	92.0 ± 3	120.59	90.5 ± 6	120.61	77.7 ± 5
130	130.46	76.2 ± 2	130.49	92.9 ± 3	130.52	109 ± 3	130.54	85.3 ± 3
140	140.38	71.5 ± 3	140.41	95.1 ± 4	140.44	115 ± 4	140.46	77.1 ± 4
150	150.30	66.0 ± 3	150.32	91.0 ± 3	150.34	99.3 ± 3	150.35	76.4 ± 4
160	160.20	61.5 ± 3	160.22	93.4 ± 5	160.23	108 ± 5	160.24	82.0 ± 6
				4.5 MeV				
20	20.21	51.5 ±14	20.23	74.3 ±14	20.24	6.25 ± 4	20.25	28.8 ±14
30	30.31	56.1 ± 5	30.33	115 ± 6	30.35	12.8 ± 4	30.36	47.8 ±15
40	40.40	92.2 ± 5	40.43	126 ± 6	40.45	28.1 ± 6	40.47	59.5 ±12
50	50.47	154.3 ± 5	50.51	105 ± 5	50.54	67.2 ± 6	50.56	106 ±30
60	60.54	216 ± 4	60.57	81.9 ± 5	60.61	116 ± 7	60.63	72.8 ± 9
70	70.58	203 ± 4	70.62	109 ± 5	70.66	147 ± 6	70.68	84.4 ± 7
80	80.61	174 ± 5	80.65	184 ± 7	80.68	175 ± 7	80.71	103 ±13
90	90.62	156 ± 4	90.66	233 ± 5	90.70	172 ± 6	90.73	142 ± 8
100	100.61	171 ± 4	100.65	246 ± 5	100.69	207 ± 8	100.71	178 ± 8
110	110.58	179 ± 4	110.62	214 ± 5	110.66	210 ± 8	110.68	178 ± 7
120	120.54	193 ± 4	120.57	196 ± 5	120.61	245 ± 8	120.63	170 ± 6
130	130.47	177 ± 4	130.51	171 ± 4	130.54	250 ± 7	130.56	161 ± 7
140	140.40	159 ± 4	140.43	179 ± 5	140.45	236 ± 8	140.47	158 ± 7
150	150.31	144 ± 4	150.33	172 ± 5	150.35	226 ± 8	150.36	156 ± 7
160	160.21	133 ± 4	160.23	182 ± 4	160.24	238 ± 6	160.25	148 ± 6
				5.0 MeV				
20	20.22	99.4 ± 9	20.23	196 ±19	20.24	13.6 ± 8	20.25	44.6 ±23
30	30.32	117 ±14	30.34	301 ±19	30.36	24.6 ± 9	30.37	93.7 ±45
40	40.41	207 ± 8	40.44	316 ±14	40.46	82.0 ±11	40.48	157 ±70
50	50.49	347 ±13	50.52	233 ±15	50.55	143 ±14	50.57	163 ±50
60	60.55	427 ± 9	60.59	165 ±10	60.62	275 ±11	60.64	150 ±13
70	70.60	434 ±11	70.64	145 ±11	70.67	327 ±12	70.70	177 ± 8
80	80.63	338 ± 8	80.67	388 ± 9	80.70	359 ±13	80.73	213 ± 8
90	90.64	288 ±10	90.68	476 ±11	90.71	351 ±18	90.74	275 ±12
100	100.63	339 ± 8	100.67	469 ±11	100.70	404 ±17	100.73	301 ±13
110	110.60	355 ± 8	110.64	370 ±11	110.67	412 ±15	110.69	286 ±14
120	120.55	354 ± 8	120.59	325 ±11	120.62	461 ±15	120.64	275 ±16
130	130.49	334 ± 8	130.57	273 ± 9	130.55	428 ±16	130.57	243 ±14
140	140.41	297 ± 8	140.44	270 ± 8	140.46	423 ±17	140.47	216 ±12
150	150.32	257 ± 9	150.34	265 ±12	150.36	286 ±32	150.37	194 ±21
160	160.22	249 ± 7	160.23	278 ± 8	160.24	360 ±19	160.25	202 ±16

TABLE I. (*continued*).

Lab angle	Ground state Center-of-mass angle	Cross section	Second excited state Center-of-mass angle	Cross section	Sixth excited state Center-of-mass angle	Cross section	Eighth excited state Center-of-mass angle	Cross section
				5.5 MeV				
20	20.22	194 ±42	20.24	362 ±60	20.25	11.5 ± 6	20.26	124 ±40
30	30.33	216 ±21	30.35	548 ±25	30.36	74 ±20	30.37	220 ±65
40	40.42	410 ±13	40.44	587 ±27	40.47	170 ±23	40.48	303 ±70
50	50.50	655 ±16	50.53	401 ±27	50.56	271 ±32	50.57	224 ±70
60	60.56	763 ±15	60.60	281 ±16	60.63	388 ±24	60.65	237 ±18
70	70.61	653 ±13	70.65	403 ±18	70.68	452 ±26	70.70	217 ±20
80	80.64	529 ±10	80.68	674 ±16	80.72	472 ±26	80.74	342 ±18
90	90.65	466 ±10	90.69	768 ±18	90.73	545 ±26	90.75	420 ±20
100	100.64	497 ±10	100.68	642 ±13	100.72	576 ±14	100.74	392 ±14
110	110.61	539 ± 9	110.65	504 ±11	110.68	562 ±15	110.70	370 ±15
120	120.56	529 ±10	120.60	405 ±11	120.63	565 ±13	120.65	317 ±14
130	130.50	456 ± 9	130.53	359 ±11	130.56	583 ±14	130.57	266 ±12
140	140.42	385 ± 8	140.44	349 ±12	140.47	521 ±16	140.48	259 ±14
150	150.33	322 ± 8	150.35	352 ±11	150.36	456 ±13	150.37	214 ±14
160	160.22	305 ± 7	160.14	357 ± 9	160.25	585 ±11	160.26	203 ±14

most treatments, it will be assumed here that the residual interaction $V_{pA}-\bar{V}_{pB}$ is negligible. By expanding $\phi(r_{pB})$ and $\phi(r_{dA})$ in the region of the short-ranged function $V_{np}\phi(r_{np})$ the integration over V_{np} can be carried out to first order.[13,14] The resulting formalism will be employed here. Also, $\phi(r_{pB})$, $\phi(r_{dA})$, and $\phi(r_{nA})$ have been made to correspond to the use of nonlocal potentials[15] by the introduction of the appropriate radially dependent factor,[16]

$$1\Big/\left(1-\frac{2m}{\hbar^2}\frac{\beta^2}{4}V\right)^{1/2},$$

for each of V_p, V_d, and V_n. β is the range of the nonlocality and was chosen in each case as $\beta=0.85$ F. The transition l values are taken from Ref. 2.

The optical-model potentials used in the Schrödinger equation to obtain the proton and deuteron scattering wave functions have the Woods-Saxon form

$$-Vg(r)-iW\left(-4a\frac{dg(r)}{dr}\right)+V_c,$$

where

$$g(r)=1/\{1+\exp[(r-R)/a]\},\quad R=R_0A^{1/3},$$

and V_c is the potential due to the charge possessed by ^{90}Zr and is assumed to be homogeneously distributed within a sphere of radius R. The real potential attains its maximum at the origin and approximately half its maximum at the radius R. The imaginary potential is characterized by the parameters R' and a' and is peaked at $r=R'$, where it has the value unity. Unless otherwise stated, the form $g(r)$ for the neutron is chosen to be the same as that for the proton. The neutron potential depth V_n is adjusted to cause the neutron wave function to vanish at the origin while at the same time to have the number of nodes predicted by the shell model. A spin-orbit term is included in the neutron potential but not in the proton or deuteron potentials. At the present energies, spin-orbit coupling effects should be negligible.

In order to study the effects of eliminating stripping which arises from the interior of the nucleus, provision is made for introducing a cutoff radius R_{co} inside of which the neutron wave function is set equal to zero.

Since the correct values of the parameters are uncertain, it is of interest to determine which sets of parameters yield the best fits to the data, and for this purpose an automatic parameter-searching routine is incorporated which treats several sets of data simultaneously with the same set of parameters. Thus it seeks out the parameters which minimize the quantity $\sum_{E,Q}\chi^2(E,Q)$, where

$$\chi^2(E,Q)=\sum_\theta\left(\frac{S_c\sigma_c(\theta)-\sigma_D(\theta)}{\epsilon_R(\theta)\sigma_D(\theta)}\right),$$

and C means calculated, D denotes experimental data, σ is the differential cross section, S is the spectroscopic factor, ϵ_R is the relative cross-section error, and θ is summed over angles at 5° intervals within the angular range of the experimental data. Finally, different bombarding energies and Q values may be included simultaneously. S_c is defined as the value which minimizes $\chi^2(E,Q)$, so that, upon setting the derivative with respect to S_c equal to zero, we obtain

$$S_c=\sum_\theta\frac{\sigma_c\sigma_D}{\epsilon_R^2\sigma_D}\Big/\sum_\theta\frac{\sigma_c^2}{\epsilon_R^2\sigma_D^2}.$$

[13] P. G. A. Buttle and L. J. B. Goldfarb, Proc. Phys. Soc. (London) **83**, 701 (1964).
[14] Gy. Bencze and J. Zimanyi, Phys. Letters **9**, 246 (1964).
[15] F. Perey and B. Buck, Nucl. Phys. **32**, 353 (1962).
[16] F. Perey, in *Proceedings of the Conference on Direct Interactions and Nuclear Reaction Mechanisms*, edited by E. Clementel and C. Villi (Gordon and Breach Science Publishers, Inc., New York, 1963), p. 125.

The data for the search routine were obtained by drawing a smooth curve through the data and extracting points every 5°. The errors at even multiples of 5° were those of the actual experimental points. Errors at odd multiples of 5° were taken as the average of the two neighboring errors.

A parameter ∇V is sometimes included which relates the potential V and the particle energy E by the equation

$$V=V_0+(\nabla V)E.$$

The constant V_0 is always chosen such that V has the value given by the elastic-scattering results at the elastic-scattering energies. It should be noted that it is precisely V that is given in the tables of parameters.

4. RESULTS

The collection of angular distributions are shown in Figs. 4, 5, 6, and 7. The errors shown are the propagated errors arising from the total counting statistics, the uncertainty of the background subtraction (often a rather large contribution for the sixth and the eighth levels), and the error in the calculated silicon reaction subtraction wherever silicon interfered with a zirconium peak. The absolute normalization has an additional error arising from the uncertainty of the relative solid angles between detectors and monitor (1%), uncertainty of integration (1%), and uncertainty of the assumption that the elastic scattering is Rutherford scattering (3%).

A general survey of the curves shows that as one progresses from 3.5 MeV to 5.5 MeV the distributions for all the states transform from structureless distributions peaked at 180° in the manner expected of "Coulomb-stripping" reactions to curves containing strong oscillations with increasing cross sections at forward angles. The sixth level is an exception to this, maintaining very nearly the same shape for all energies.

For the 3.5 and 4.0 MeV measurements, difficulty arising from the oxygen, carbon, and silicon contaminants and excessive pulse pile-up, combined with the small zirconium reaction cross sections, prevented altogether a measurement of the sixth and eighth states at the smallest angles or else yielded a result with rather large errors.

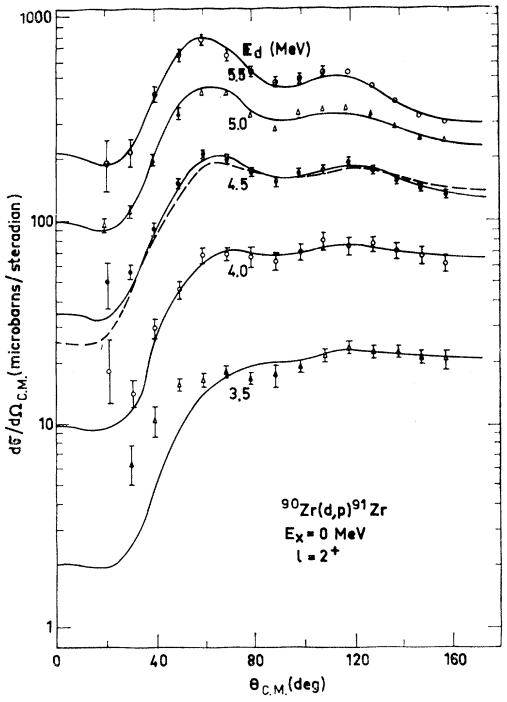

FIG. 4. Absolute differential cross sections expressed in center-of-mass system for the ^{90}Zr$(d,p)^{91}$Zr reactions leading to the ground-state of ^{91}Zr at E_d=3.5, 4.0, 4.5, 5.0, and 5.5 MeV. The theoretical curves were obtained with the aid of parameter set A of Table II and were normalized to the experimental cross sections by the spectroscopic factors listed in Table III. The dashed lines correspond to the same calculations except that $\nabla V_d=-0.4$.

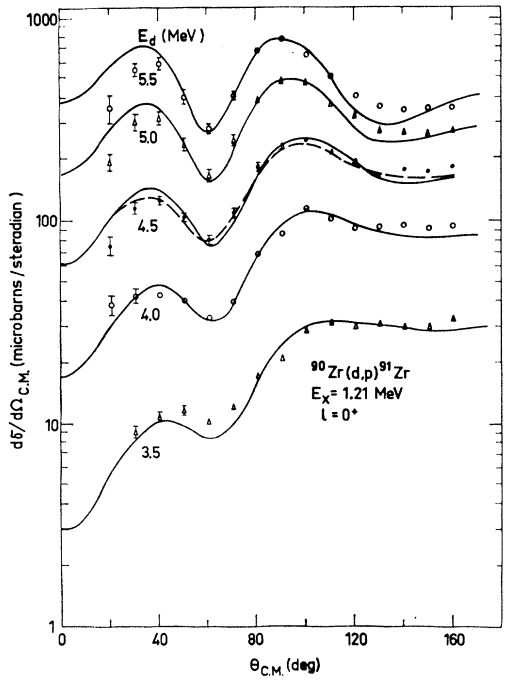

FIG. 5. Same case as Fig. 4, but for the 1.21-MeV level of ^{91}Zr.

The parameter values on which the stripping analysis is based were obtained from optical-model studies of the 11.8-MeV ^{Nat}Zr(d,d) data of Schmidt-Rohr *et al.*[17] and the 16.2 MeV ^{93}Nb(p,p) data of Fulmer.[18] [A comparison between the elastic deuteron scattering from ^{Nat}Zr and ^{90}Zr has been made.[19] No significant difference in the relative angular distribution was found; however, the measurements yielded an absolute cross section for

[17] G. Igo, W. Lorenz, and U. Schmidt-Rohr, Phys. Rev. **124**, 832 (1961).
[18] C. B. Fulmer, Phys. Rev. **125**, 631 (1962).
[19] F. Perey (unpublished).

$^{90}Zr(d,d)$ 5% less than that for $^{Nat}Zr(d,d)$.] Several sets of parameters are considered, three of these being listed in Table II. Deuteron set A was obtained by Perey[20] after varying all the parameters so as to minimize the least-squares agreement with data for a wide range of targets and energies. Proton set A employed the geometrical parameters specified by Perey[21] as the set which gave agreement with data for a wide range of targets and energies. In the present case, V and W have been optimized specifically for $^{93}Nb(p,p)$ by a search code. Parameter set A may thus be considered as the best choice for stripping studies. The other proton and deuteron parameter sets which have been employed in these calculations are listed in Table II of

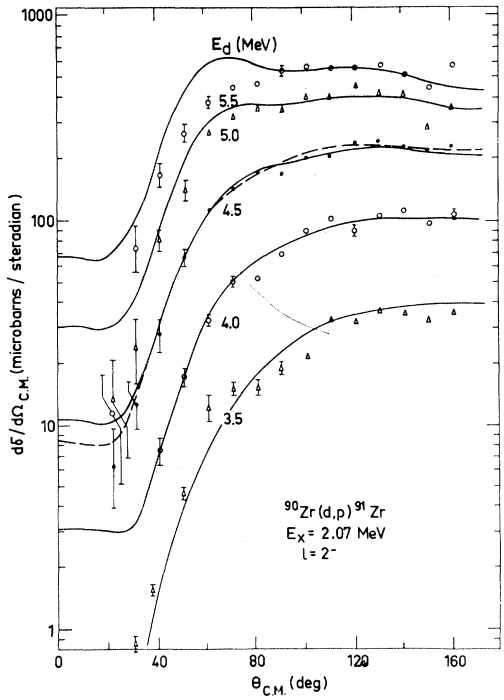

FIG. 6. Same case as Fig. 4, but for the 2.07-MeV level of ^{91}Zr.

Ref. 5, which treated the $^{90}Zr(d,p)$ reaction at $E_d=10.85$ and 15 MeV. These parameters included deuteron sets with $R_{0d}=1.1$, 1.2, and 1.3 and proton sets with $R_{0d}=1.1$, 1.2, and 1.23. The latter proton set was obtained by optimizing all the parameters, and when applied in the present study gave results little different from proton set A in Table II.

The behavior of the spectroscopic factors obtained from the $E_d=3.5$ to 5.5 MeV data was dominated by the choice of proton parameters and was relatively insensitive to the deuteron parameters, the tendency being for the spectroscopic factors to become smaller and to assume a negative energy dependence as the

[20] C. M. Perey and F. G. Perey, Phys. Rev. 132, 755 (1963).
[21] F. G. Perey, Phys. Rev. 131, 745 (1963).

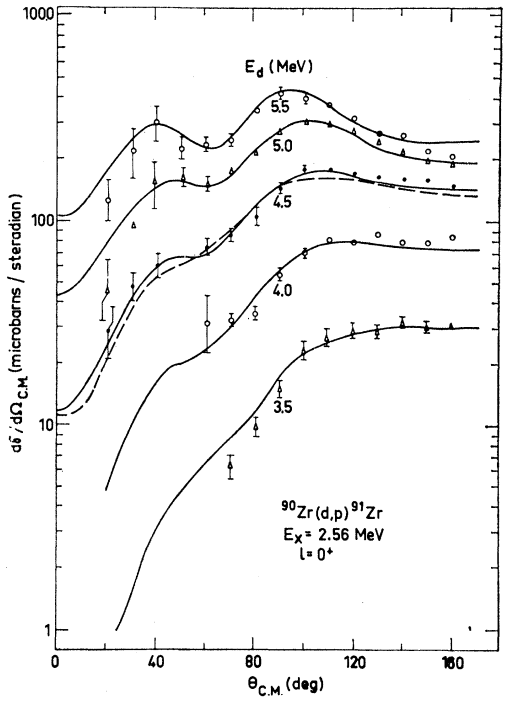

FIG. 7. Same case as Fig. 4, but for the 2.56-MeV level of ^{91}Zr.

radius is increased. As will be shown, this insensitivity feature probably arises from the convention of selecting the neutron radius and diffuseness to be identical to those for the proton. Therefore, the discussion is restricted to the parameter combinations in Table II, although additional combinations of proton and deuteron parameter sets were actually considered.

The deuteron parameters of set A were used to calculate the elastic scattering cross section to compare with the measurements made at 5.5 MeV, where the deviation from Rutherford scattering is the largest and which might give an indication of the validity of the elastic parameters at this energy. The calculation gives the dashed curve in Fig. 3 for the ratio of experimental to Rutherford cross section. The parameters yield the correct trend of the cross section, but the details do not agree with the experimental curves.

TABLE II. Parameters from 11.8-MeV Zr(d,d) and 16.2-MeV Nb(p,p) scattering.

Proton or deuteron	Set	R_0 (F)	a (F)	R_0' (F)	a' (F)	V (MeV)	W (MeV)
p	A	1.25	0.65	1.25	0.47	50.89	13.63
d	A	1.272	0.679	1.236	0.677	85.4	18.39
p	B	1.2	0.7161	1.257	0.5482	54.28	11.71
d	B	1.2	0.6809	1.260	0.8634	92.12	12.20
p	C	1.1	0.6882	1.514	0.7628	61.94	5.295
d	C	1.1	0.7329	1.361	0.8692	104.8	10.02

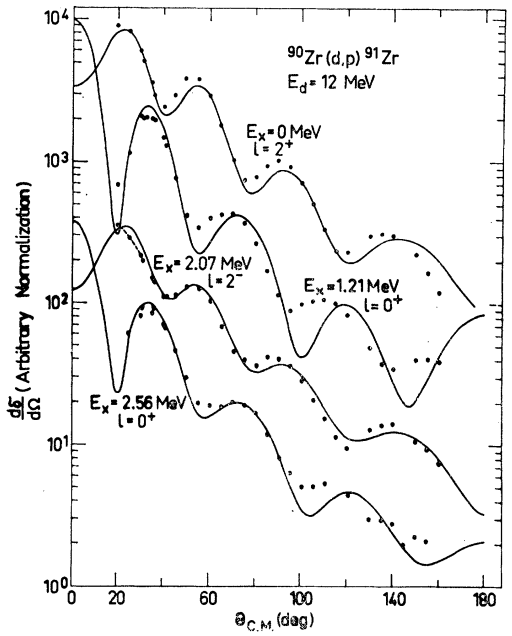

FIG. 8. Comparisons between the experimental differential cross sections obtained by Dickens *et al.* (Ref. 4), for the $E_d=12$ MeV, ^{90}Zr$(d,p)^{91}$Zr reactions leading to the ground, 1.21-, 2.07-, and 2.56-MeV levels of ^{91}Zr, and calculations employing elastic-scattering parameter set *A* of Table II.

The results of performing stripping calculations with parameter set *A* are compared in Figs. 4, 5, 6, and 7 with the $E_d=3.5$ to 5.5 MeV stripping angular distributions and in Fig. 8 with the 12-MeV stripping data. The

TABLE III. Spectroscopic factors, averages, and percent deviations corresponding to the parameter sets in Table II with $\nabla V_p=-0.5$ MeV.

Set	E_d (MeV)	E_x (MeV) 0 S	$\%D$[a]	1.21 S	$\%D$	2.07 S	$\%D$	2.56 S	$\%D$
A	3.5	0.64	7	0.55	6	0.49	11	0.168	6
	4.0	0.62	3	0.57	10	0.44	0	0.163	3
	4.5	0.61	2	0.52	0	0.44	0	0.168	6
	5.0	0.58	−3	0.50	−4	0.43	−2	0.153	−4
	5.5	0.53	−12	0.47	−10	0.41	−7	0.141	−11
	S_{av}[b]	0.60		0.52		0.44		0.159	
	12	0.61	2	0.55	6	0.45	2	0.186	17
B	3.5	0.75	1	0.60	0	0.52	4	0.178	1
	4.0	0.74	0	0.63	5	0.49	−2	0.176	−1
	4.5	0.75	1	0.60	0	0.50	0	0.189	1
	5.0	0.75	1	0.60	0	0.50	0	0.174	−2
	5.5	0.70	−5	0.58	−3	0.50	0	0.168	−5
	S_{av}	0.74		0.60		0.50		0.177	
	12	0.78	5	0.65	9	0.55	10	0.218	23
C	3.5	1.42	−6	0.98	−5	0.88	−3	0.277	−4
	4.0	1.44	−5	1.07	4	0.86	−5	0.282	−2
	4.5	1.53	1	1.02	−1	0.91	0	0.301	1
	5.0	1.58	5	1.04	1	0.94	3	0.289	0
	5.5	1.56	3	1.05	2	0.97	1	0.285	−1
	S_{av}	1.51		1.03		0.91		0.288	
	12	1.60	6	1.28	24	1.40	54	0.484	68

[a] $\%D=100(S-S_{av})/S_{av}$.
[b] $S_{av}=(S_{3.5}+S_{4.0}+S_{4.5}+S_{5.0}+S_{5.5})/5$.

TABLE IV. Least-squares fit to all the $E_d=3.5$ to 5.5 MeV data.

Parameter set	$\chi/N^{1/2}$ [a]
A	2.25
A, $\Delta V_d=-0.4$ MeV	2.06
A, best relative fit parameters	1.85
B	2.58
C	2.83

[a] N is the sum total of the number of angles at all energies and for all levels for which data were included in the search code.

corresponding spectroscopic factors are listed in Table III. In these calculations the proton potential has a linear energy dependence of $\nabla V_p=-0.5$ as suggested by Perey's proton elastic-scattering analysis.[21] In accordance with Perey's deuteron scattering analysis[20] an energy dependence of $\nabla V_d=-0.4$ was also tried for the deuteron channel with almost no change in the spectroscopic factors but with a slight increase in the quality of the fits as indicated by the corresponding χ in Table IV. Examples for $E_d=4.5$ MeV are shown as dashed lines in Figs. 4, 5, 6, and 7.

Since there is uncertainty about how the extrapolation of the parameters should be made between the elastic-scattering energy and the energies of this stripping analysis, an investigation has been made into whether or not other parameter sets exist in the neigh-

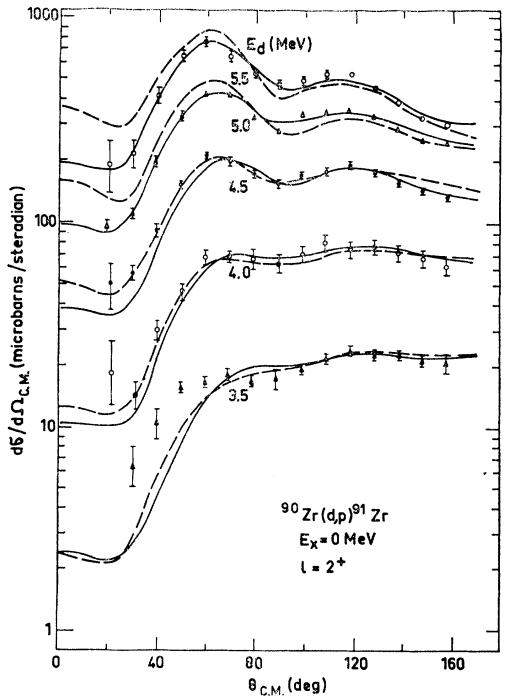

FIG. 9. Comparisons between experimental differential cross sections for the ^{90}Zr$(d,p)^{91}$Zr reactions leading to the ground state of ^{91}Zr at $E_d=3.5$, 4.0, 4.5, 5.0, and 5.5 MeV and the results of DWBA calculations in which (solid curves) the parameters in Table V have been employed and (dashed curves) parameter set *C* in Table II was used.

TABLE V. Best-relative-fit stripping parameters employing form-factor set A.

V_p (MeV)	∇V_p	W_p (MeV)	V_d (MeV)	W_d (MeV)
56.87	−0.55	13.63	88.73	12.13

borhood of the elastic parameters which yield significant improvement in the results. Employing the geometrical parameters of set A, repeated grid-type searches on V_p, V_d, W_p, and W_d, followed by automatic search on V_p, V_d, and W_d (the calculations proved to be relatively insensitive to W_p), produced the parameters listed in Table V and the corresponding fits shown in Figs. 9, 10, 11, and 12. For the most part there is little reason to prefer these new results to the previous ones. All the improvement appears to be restricted to the 1.21- and 2.07-MeV levels. Part of the discrepancy may lie in the data, since the 2.07-MeV-level data probably contain a contribution from the unresolved seventh level. The new spectroscopic factors are in general about 7% smaller than before and have an even more severe energy dependence.

Of all the parameter sets considered, set C produced the largest χ. The results are plotted as dashed lines in Figs. 9–12, and are seen to be still in relatively good agreement with the data. It should be pointed out that of the parameters considered here these parameters gave the worst fits to the proton and deuteron elastic scattering, and to the 12-MeV stripping data (the ratio of χ for parameter set C to that for set A is 1.66) and that also $\nabla V_p = -0.5$ is a rather arbitrary choice for the energy dependence of the proton potential when $R_{0p} = 1.1$.

The Coulomb repulsion of the deuterons due to their low energy should cause a relatively greater percentage

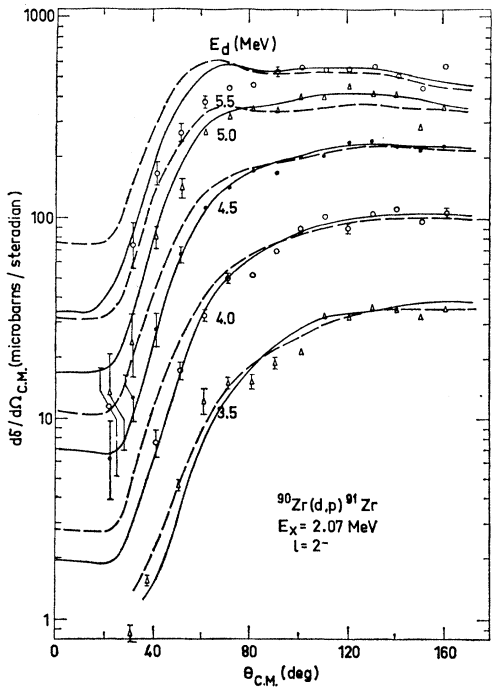

FIG. 11. Same case as Fig. 9, but for the 2.01-MeV level of ^{91}Zr.

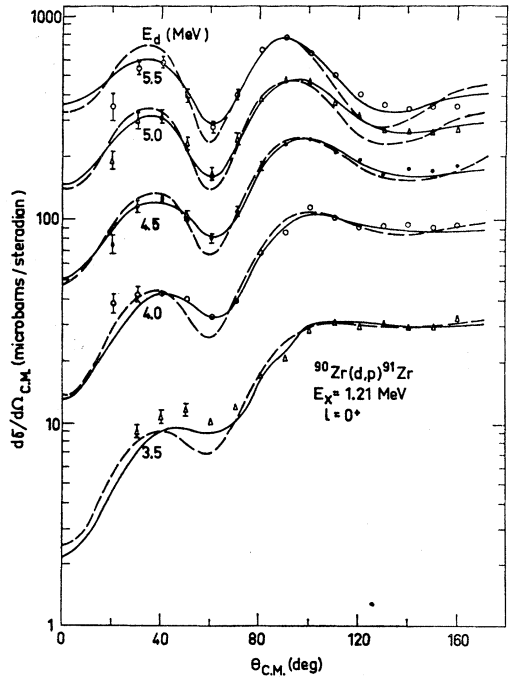

FIG. 10. Same case as Fig. 9, but for the 1.21-MeV level of ^{91}Zr.

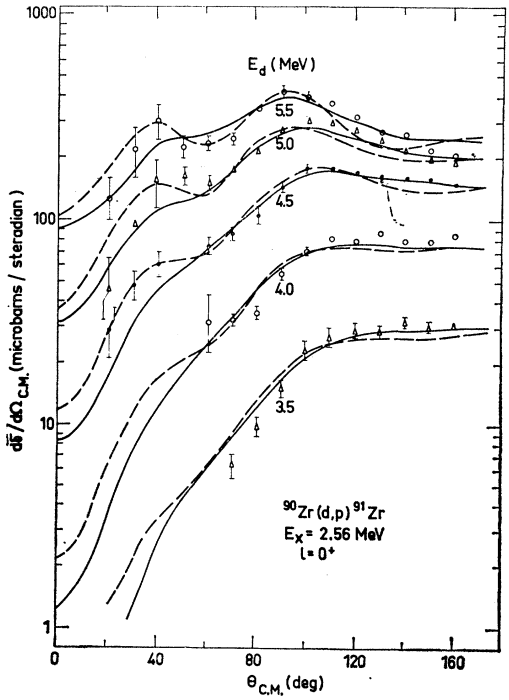

FIG. 12. Same case as Fig. 9, but for the 2.56-MeV level of ^{91}Zr.

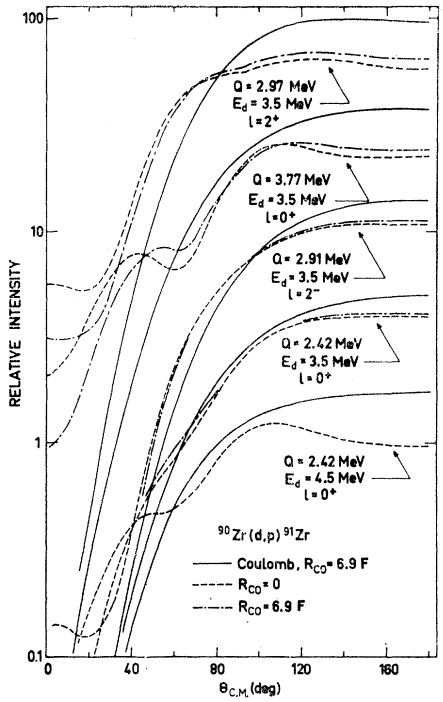

FIG. 13. Coulomb-stripping calculations and also DWBA calculations with and without a radial cutoff. For the Coulomb-stripping curves the nuclear potentials have been set equal to zero. The other curves are calculated with parameter set A. The ordinates give the relative values for each set of curves.

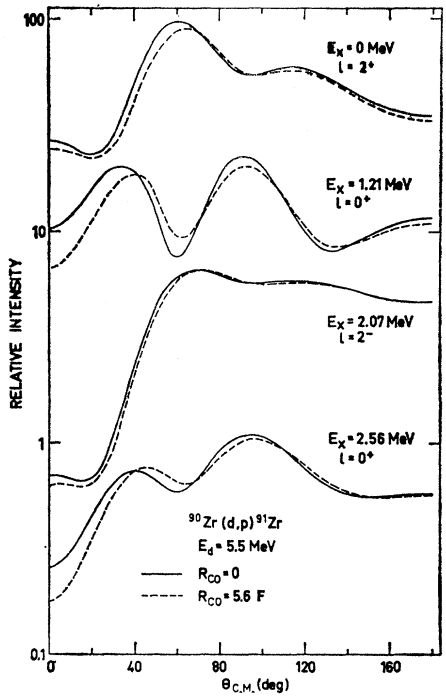

FIG. 14. DWBA calculations employing parameter set A with and without a radial cutoff. The ordinates give the relative values for each set of curves.

of the stripping to occur in the "tail" of the target density. To investigate this possibility, cutoff radii were introduced into the calculations of the radial integrals, thus effectively eliminating stripping contributions from the nuclear interior. The results of using cutoffs are shown in Fig. 13 for $E_d=3.5$ MeV and $R_{co}=R_n+2a_n$ and in Fig. 14 for $E_d=5.5$ MeV and $R_{co}=R_n$. The radii chosen represent those for which the cutoff effects begin to become noticeable at the respective energies. Thus at $E_d=3.5$ MeV the effects of a cutoff are negligible when $R_{co}=R_n$. Also shown in Fig. 13 are results obtained by using a cutoff and also setting the optical-model potentials equal to zero, a situation known as Coulomb stripping.

Finally, to illustrate that relative comparisons of spectroscopic factors have more meaning than their absolute magnitudes, some calculations with parameter set A were performed for the transition leading to the ^{91}Zr ground state in which R_{0n} was varied by ± 0.1 F and a_n by ± 0.2 F. With these magnitudes the effects, both on the shapes and magnitudes of the differential cross sections, of varying R_{0n} were almost identical to the effects of varying a_n. The shapes were affected only a little; however, the magnitudes changed by factors of $(1.52)^{\pm 1}$ at $E_d=5.5$ MeV and $(1.45)^{\pm 1}$ at $E_d=12$ MeV.

5. DISCUSSION

The results described in the previous section indicate that the distorted-wave Born approximation is valid for calculating the relative angular distributions for the stripping reaction but unreliable for calculating absolute magnitudes. Thus, the angular shapes depended little on whether parameter set A, B, C, or some other set was employed or whether or not the deuteron potential was energy-dependent. In fact, at lower bombarding energies and higher excitations the distributions tended to be wholly indifferent to parameters. Because the nuclear interior contributes little to the stripping, the results should not depend on which of the many possible sets of parameters agreeing with the elastic-scattering data are used in the stripping calculations, especially since the elastic scattering is determined only by the asymptotic forms of the wave functions. In addition, the straightforward use of elastic-scattering parameters gave agreement with the experimental angular shapes not notably inferior to the agreement obtained after a more thorough variation of the parameters.

On the other hand, as seen in Table III, the best set of parameters, set A, yields spectroscopic factors which exhibit an unacceptably large dependence on energy. This is untenable. Actual spectroscopic factors are intrinsically independent of bombarding energy. The normalizations of the calculations to the data are somewhat arbitrary but not enough to remove all of the

energy dependence. It is possible that the spectroscopic-factor behavior is due to a neglect of the residual interaction in the stripping matrix element.[21] Neglect of this interaction should not seriously affect the shapes of the angular distributions but would be expected to produce energy-dependent spectroscopic factors since, of course, the wave functions are themselves energy-dependent.

The spectroscopic factors are definitely smaller in the case of the ground state and 1.21-MeV level transitions than the values 0.98 and 0.96, respectively, which are predicted by shell-model calculations.[6] These calculations assumed ^{90}Zr to be a ^{88}Sr closed shell plus 3 nucleons. This discrepancy can be removed by decreasing the radius and diffuseness of the neutron potential. Because the proton and neutron potentials are expected to be similar, this implies that the proton radius should be smaller. Indeed, parameter sets B and C with $R_{op}=R_{0n}=1.2$ and 1.1, respectively, exhibit some improvements in the spectroscopic factors (see Table III). Those for $R_{op}=1.2$ are nearly constant and also somewhat larger than for set A. For $R_{op}=1.1$, the spectroscopic factors are actually too large and an energy dependence appears which is the reverse of what it was for parameter set A. Supposedly, for $R_{op}\approx 1.15$ the spectroscopic factors would exhibit little energy dependence and also have about the right magnitudes. Such a radius may be allowable since it has never been demonstrated that a proton elastic-scattering study with this radius would not yield agreement with a large range of energies and targets similar to the consistent results obtained with $R_{op}=1.25$. However, the results obtained with parameter sets B and C do have faults. The ratio of the ground to the 1.21-MeV level spectroscopic factors has become undeniably too large when $R_{op}=1.1$. Also, the spectroscopic factors at 12 MeV have become larger than those obtained at 3.5 to 5.5 MeV.

The cutoff and Coulomb-stripping results illustrated in Figs. 13 and 14 show that the stripping is largely independent of events occurring in the nuclear interior and that the Coulomb-stripping region is approached, but not quite reached, when $E_d=3.5$ MeV and $Q<3$ MeV. Taking account of the fact that the nuclear interior becomes less important as Q is lowered it is seen that, other things being equal, the $l=2$ reactions occur less in the nuclear interior than the $l=0$ ones, which seems reasonable because $l=0$ reactions classically correspond to reactions initiated by deuterons colliding head-on with the target. Because elastic scattering is determined fully by the shapes of the exterior wave functions, the stripping results, being dependent themselves mostly on the exterior wave functions, should be largely independent of the choice of equally valid elastic-scattering parameters. Thus, the relatively good fits to the experimental angular distributions shown in Figs. 4–7 do not result from an accidently favorable choice of parameters.

[22] B. Buck and J. R. Rook, Nucl. Phys. **67**, 504 (1965).

6. CONCLUSIONS

For future experiments of this sort one should emphasize three requirements for performing successful experiments. These should include targets of very high purity, free from low-Z contaminants, thin targets of the order $\frac{1}{2}$ mg/cm^2, and very uniform absorbers. Fulfillment of any two of the above three requirements would reduce the importance of the remaining one.

This work is the first attempt to fit deuteron stripping data and extract spectroscopic factors with the DWBA analysis with such a heavy mass and low range of energies. The analysis has shown that the DWBA employing the elastic-scattering parameters obtained at higher energies correctly predicts the main features of (d,p) angular distributions when the bombarding energy is about half the deuteron Coulomb-barrier energy and that this agreement is not due to a fortuitous choice of parameters because the predicted results are both relatively parameter-insensitive and do not depend much on the shapes of the wave functions in the nuclear interior. It is very satisfying to note that the same parameters and analysis fit very nicely the forward-peaked angular distributions at 12 MeV and the backward-peaked angular distributions in the range 3.5–5.5 MeV, where at the lower energy the Coulomb-stripping region is approached. However, the theory is less satisfactory for predicting spectroscopic factors, because these are found to be quite dependent on the choice of potential parameters. In fact, they are both energy-dependent and incorrect in magnitude when the most justifiable set of parameters is employed. Whether this is a defect in the stripping theory or in the prescription for choosing the parameters remains to be seen.

ACKNOWLEDGMENTS

Two of us (E.D. and J.N.) thank the Institute de Recherches Nucléaires, Strasbourg, for the hospitality and facilities offered to us during the period in which this work was completed. We are grateful to R. Tapiero for his aid in data taking. We thank Dr. E. Hudspeth for generously furnishing the target to us, and making available the thesis results of D. Goss. Finally, we are indebted to Dr. J. K. Dickens for allowing us the use of the unpublished 12-MeV $^{90}Zr(d,p)^{91}Zr$ data.